Inorganic Chemistry

Article

pubs.acs.org/IC

Ferromagnetic Coupling in "Double-Bridged" Dihydrogenpyrophosphate Complexes of Cobalt(II) and Nickel(II)

Tiffany J. Greenfield,[†] Amanda E. Hoffman,[†] Nadia Marino,[†,§] Alan G. Goos,[†,⊥] Francesc Lloret,[‡] Miguel Julve,*[,‡] and Robert P. Doyle*[,†]

[†]Department of Chemistry, Syracuse University, Syracuse, New York 13244-4100, United States

[‡]Departament de Quimica Inorganica/Instituto de Ciencia Molecular, Facultat de Química, Universitat de València, Catedratico Jose Beltran 2, 46980 Paterna, Valencia, Spain

Supporting Information

ABSTRACT: Three isostructural compounds of the formula $\{[M(bipy)(H_2O)(H_2P_2O_7)]_2\cdot 2H_2O\}$ [bipy = 2,2′-bipyridine; M = Ni (**1**), Co (**2**), Mn (**3**)] have been isolated from aqueous solutions containing the corresponding metal(II) chloride hydrate with a bipy and sodium pyrophosphate solution in a 1:1:2 molar ratio, and their structures were determined by single-crystal X-ray diffraction. The structures of **1**−**3** consist of neutral aqua(2,2′-bipyridine)metal(II) dinuclear units bridged by two dihydrogenpyrophosphate groups adopting a bidentate/monodentate mode. Each metal ion in **1**−**3** is six-coordinate in a distorted octahedral geometry, with the reduced value of the angle subtended by the chelating bipy at the metal ion [79.6(1)° (**1**), 77.32(7)° (**2**), and 72.9(1)° (**3**)] being the main source of this distortion. The values of the intramolecular metal−metal separation are 5.271(1) Å (**1**), 5.3065(8) Å (**2**), and 5.371(1) Å (**3**). Magnetic susceptibility measurements on polycrystalline samples of **1**−**3** in the temperature range 1.9−300 K shows weak intramolecular ferromagnetic [J = +1.86(2) cm^{-1} (**1**) and +0.25(1) cm^{-1} (**2**)] and antiferromagnetic [J = −0.48(1) cm^{-1} (**3**)] coupling, with the spin Hamiltonian being defined as $\boldsymbol{H} = -J\boldsymbol{S}_{M1}\cdot\boldsymbol{S}_{M1a}$. This rarely observed coordination mode for dihydrogenpyrophosphate leads to ferromagnetic coupling in complexes of nickel(II) or cobalt(II).

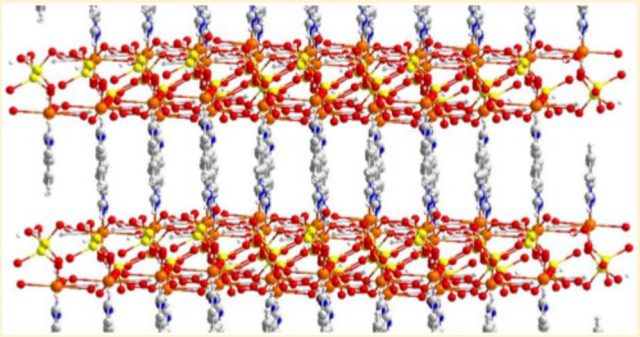

INTRODUCTION

Inorganic pyrophosphate (PPi; $P_2O_7^{4-}$) is a tetraanion composed of two inorganic phosphate (Pi) molecules linked by a hydrolyzable ester bond.[1,2] PPi is involved in biological processes including adenosine triphosphate production, energy storage,[3−7] and the development of mineralized tissues.[8] PPi has also been shown to inhibit vascular calcification.[9−11] Misregulation of the cellular levels of PPi has been associated with diseases such as Pseudoxanthoma elasticum (PXE).[1,12] The metal-binding properties of PPi salts and their properties (magnetic, biological, materials, catalytic, etc.) have been a source of considerable research efforts over recent years.[13,14] The great majority of the PPi coordination complexes reported to date have contained single PPi units, bridging or terminal (see Scheme 1a−g), with the incorporation of multiple bridging PPi units between metal centers in a single complex, and the effects thereof, systematically unexplored to date.

We therefore decided to attempt to synthesize coordination complexes with first-row transition-metal ions incorporating at least two PPi units bridging across paramagnetic metal centers and focus on the magnetic properties inherent in such an arrangement. The magnetic properties of PPi complexes to date have primarily exhibited antiferromagnetic interactions,[15−18] with only one example of ferromagnetic coupling reported to date (of the 36 magnetically characterized PPi-bridged complexes), namely, the copper(II) complex of the formula $\{[Cu(bipy)(cis\text{-}H_2P_2O_7)]_2\}\cdot 3H_2O$ (**4**) with bipy = 2,2′-bipyridine [J = +0.86(1) cm^{-1}, with the Hamiltonian being defined as $H = -JS_{Cu1}\cdot S_{Cu1a}$].[19]

The successful outcomes of this work are borne in the synthesis of three new isostructural complexes characterized by single-crystal X-ray diffraction studies that contain two $H_2P_2O_7^{2-}$ anions exhibiting the bidentate/monodentate bridging mode (**h** in Scheme 1). They connect two metal ions [nickel(II), cobalt(II), or manganese(II)] within a single homodinuclear complex with the bipy molecule as end-cap ligands. Variable-temperature magnetic susceptibility measurements of these three dinuclear compounds, namely, $[Ni(bpy)(H_2P_2O_7)(H_2O)]_2\cdot 2H_2O$ (**1**), $[Co(bpy)(H_2P_2O_7)(H_2O)]_2\cdot 2H_2O$ (**2**), and $[Mn(bpy)(H_2P_2O_7)(H_2O)]_2\cdot 2H_2O$ (**3**), revealed ferromagnetic interactions for dihydrogenpyrophosphate-containing complexes of nickel(II) and cobalt(II).

Received: April 16, 2015
Published: June 23, 2015

DOI: 10.1021/acs.inorgchem.5b00866
Inorg. Chem. 2015, 54, 6537−6546

Scheme 1. Coordination Modes of the Pyrophosphate Ligand That Have Been Observed to Date in Discrete Coordination Complexes[a]

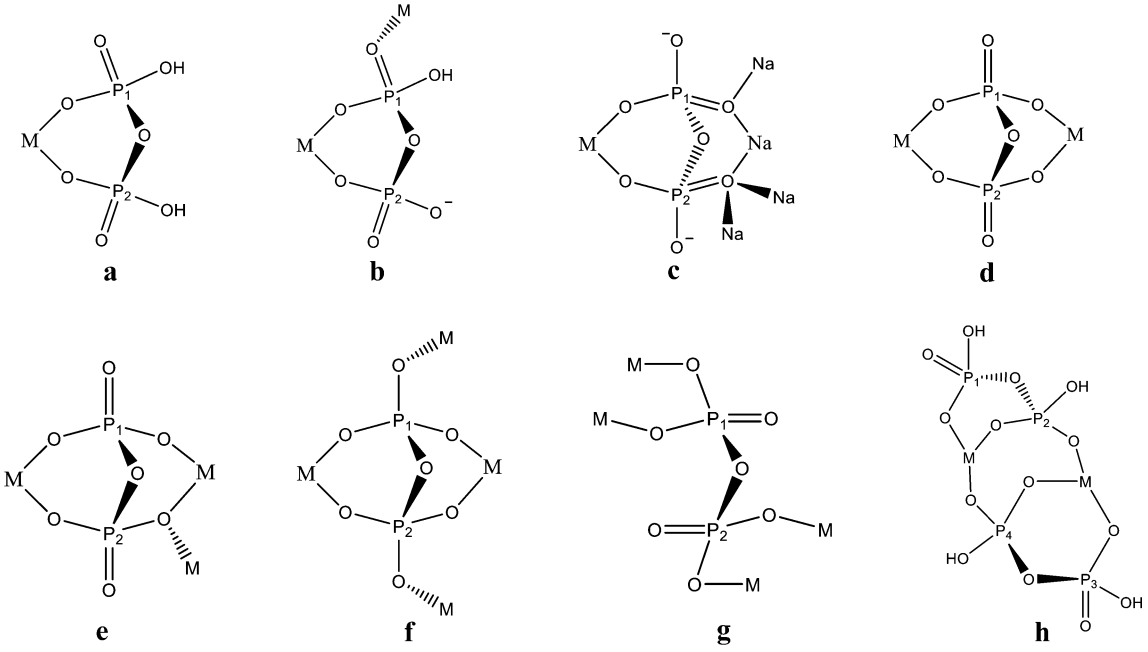

[a]**a** and **d** are the classical bidentate and bis-bidentate coordination modes respectively, whereas **h** shows the double bidentate/monodentate bridging mode, which was observed for the first time in $\{[Cu(bipy)(cis\text{-}H_2P_2O_7)]_2\}\cdot 3H_2O$ (**4**) and $\{[Cu(bipy)(trans\text{-}H_2P_2O_7)]_2\}$[19] and in complexes **1**−**3** described herein.

Table 1. Summary of Crystallographic Data for 1−3

	1	2	3
CCDC number	1046979	1046977	1046978
chemical formula	$Ni_2C_{20}N_4H_{28}P_4O_{18}$	$Co_2C_{20}N_4H_{28}P_4O_{18}$	$Mn_2C_{20}N_4H_{28}P_4O_{18}$
M	853.76	854.20	846.22
cryst syst	triclinic	triclinic	triclinic
space group	$P\bar{1}$	$P\bar{1}$	$P\bar{1}$
a/Å	8.0187(15)	8.0269(11)	8.065(2)
b/Å	9.4817(18)	9.6018(13)	9.770(3)
c/Å	10.757(2)	10.8292(15)	10.970(3)
α/deg	83.110(4)	83.373(3)	84.004(6)
β/deg	79.799(4)	79.281(3)	78.651(5)
γ/deg	67.755(4)	67.531(2)	66.716(6)
V/Å^3	743.8(2)	756.91(8)	778.1(3)
Z	1	1	1
D_c/(g cm^{-3})	1.906	1.874	1.806
T/K	90(2)	90(2)	90(2)
μ(Mo Kα)/mm^{-1}	1.572	1.383	1.104
F(000)	436	434	430
cryst size max/mm	0.40−0.50	0.31−0.45	1.00−1.50
cryst size mid/mm	0.30−0.45	0.21−0.40	0.21−0.30
cryst size min/mm	0.19−0.35	0.15−0.19	0.19−0.20
no. of reflns measd	18751	25510	14935
no. of indep reflns	3010	4390	4281
GOF on F^2	1.099	0.978	1.119
$R1$, $wR2$ [$I > 2\sigma(I)$]	0.0303, 0.0928	0.0369, 0.0758	0.0392, 0.1236
$R1$, $wR2$ (all data)	0.0362, 0.0997	0.0625, 0.0828	0.0466, 0.1336
$\Delta\rho_{max}$, $\Delta\rho_{min}$/(e Å^{-3})	0.494, −0.451	0.526, −0.411	0.817, −0.639

EXPERIMENTAL SECTION

General Procedures. Solvents and reagents were purchased from Sigma-Aldrich and used as received. Water was distilled and deionized (DI) to 18.6 MΩ using a Barnstead Diamond RO reverse-osmosis machine coupled to a Barnstead Nano Diamond ultrapurification machine. Elemental analyses (C, H, and N) were completed by QTI Intertek, Whitehouse, NJ. Centrifugation for both syntheses was carried out using a Sorvall RT machine at a speed of 4000 rpm at room temperature for 10 min. IR spectra were collected on a Nicolet Magna-

DOI: 10.1021/acs.inorgchem.5b00866
Inorg. Chem. 2015, 54, 6537−6546

IR 850 series II spectrophotometer as KBr pellets. Thermogravimetric analysis was completed using a TA Instruments Q50 analyzer, typically using 5.0 mg samples placed on a platinum pan under a dinitrogen atmosphere at a flow rate of 20 mL min^{-1}. The temperature was ramped from ca. 25 to 500 °C at a rate of 10 °C min^{-1}. Spectral analysis was performed on TA Instruments *Universal Analysis 2000* software. Magnetic susceptibility measurements on polycrystalline samples of **1**−**3** were carried out on a Quantum Design SQUID magnetometer in the temperature range 1.9−300 K operating at 1000 G ($T \geq 50$ K) and 250 G ($T < 50$ K). The magnetization measurements were performed at 2.0 K in the field range 0−5 T. Corrections for the diamagnetic contribution of the constituent atoms were estimated from Pascal's constants[20] as -438×10^{-6} cm^3 mol^{-1} K (**1** and **2**) and -442×10^{-6} cm^3 mol^{-1} K (**3**) [per two metal(II) ions]. The values of the experimental magnetic susceptibilities were also corrected for temperature-independent paramagnetism and the sample holder (a plastic bag).

Synthesis of the Complexes. [Ni(bpy)($H_2P_2O_7$)(H_2O)]$_2$·2H_2O (1). Nickel(II) chloride hexahydrate (0.0951 g, 0.4 mmol) and bipy (0.0625 g, 0.4 mmol) were added to DI water (10 mL) with stirring. A solution of sodium pyrophosphate (0.2127 g, 0.8 mmol) in 5 mL of DI water was then added. The pH of the solution was lowered to pH 2.0 from pH 9.6 using 1 M HCl. The gray solution was allowed to stand at room temperature, where green block crystals formed after 4 days. The final mass of the crystals after drying for 3 days in vacuo was 0.0444 g. The yield based on bipy was 26%. Elem anal. Calcd for $C_{20}H_{28}N_4Ni_2O_{18}P_4$ (**1**; MW = 853.72 g mol^{-1}): C, 28.14; H, 3.30; N, 6.56. Found: C, 28.01; H, 3.18; N, 6.48. FT-IR (KBr, cm^{-1}): 3448(br), 1601(m), 1445(s), 1255(s), 1176(m), 1156(w), 1113(m), 1051(w), 1028(s), 996(s).

[Co(bpy)($H_2P_2O_7$)(H_2O)]$_2$·2H_2O (2). Cobalt(II) chloride hexahydrate (0.0952 g, 0.4 mmol) and bipy (0.0625 g, 0.4 mmol) were added to DI water (10 mL) with stirring. Sodium pyrophosphate (0.2127 g, 0.8 mmol) was dissolved in 5 mL of DI water and then added to the previous solution. The pH was adjusted from pH 9.8 to pH 2.0 by using 1 M HCl. The pink solution was allowed to stand at room temperature, whereupon pink block crystals suitable for X-ray diffraction studies formed within 24 h. The final mass of the crystals after drying for 3 days in vacuo was 0.1308 g. The yield based on bipy was 76%. Elem anal. Calcd for $C_{20}H_{28}N_4Co_2O_{18}P_4$ (**2**; MW = 854.20 g mol^{-1}): C, 28.12; H, 3.30; N, 6.56. Found: C, 28.14; H, 3.18; N, 6.50. FT-IR (KBr, cm^{-1}): 3448(br), 1599(m), 1443(m), 1253(s), 1176(m), 1156(m), 1114(m), 1053(s), 998(m).

[Mn(bpy)($H_2P_2O_7$)(H_2O)]$_2$·2H_2O (3). Manganese(II) chloride tetrahydrate (0.0792 g, 0.4 mmol) and bipy (0.0625 g, 0.4 mmol) were added to DI water (10 mL) with stirring. A solution of sodium pyrophosphate (0.2127 g, 0.8 mmol) in 5 mL of DI water was then added. The pH of the solution was lowered to pH 2.0 from pH 9.8 using 1 M HCl. The light-pink solution yielded yellow needles formed after standing at room temperature for 72 h. The final mass of the crystals after drying for 3 days in vacuo was 0.0484 g. The yield based on the starting metal salt was 28%. Elem anal. Calcd for $C_{20}H_{28}N_4Mn_2O_{18}P_4$ (**3**; MW = 846.21 g mol^{-1}): C, 28.39; H, 3.34; N, 6.62. Found: C, 28.53; H, 2.89; N, 6.52. FT-IR (KBr, cm^{-1}): 3448(br), 1600(s), 1442(s), 1244(s), 1184(s), 1153(s), 1037(s), 996(s).

Structure Determination and Refinement of 1−3. X-ray crystallographic data for **1**−**3** were collected with a Bruker Apex II CCD diffractometer using graphite-monochromated Mo Kα radiation (λ = 0.71073 Å) at a temperature of 90 K. Data collection and cell refinement were performed through the *APEX2* suite.[21] Data were processed through the *SAINT*[22] reduction and *SADABS*[23] (for **2**) or *TWINABS*[24] (for twinned crystals of **1** and **3**) absorption software. A summary of the crystallographic data and structure refinement for the three compounds is given in Table 1. The structures were solved by direct methods, subsequently completed by Fourier recycling using the *SHELXTL-2013* software package,[25] and then refined by the full-matrix least-squares refinements based on F^2 with all observed reflections. All non-hydrogen atoms were refined anisotropically. The hydrogen atoms of the $H_2P_2O_7^{2-}$ group as well as those of the bipy molecule were placed on calculated positions and refined using a riding model. The hydrogen atoms of the coordinated and crystallization water molecules were located from the Fourier difference map and refined with restraints on the O−H and H···H distances. The main bond lengths and angles for **1**−**3** are shown in Table 2. CCDC reference numbers are 1046979 (**1**), 1046977 (**2**), and 1046978 (**3**).

Table 2. Selected Bond Lengths (Å) and Angles (deg) and Metal−Metal Separation Values for 1−3[a] [M = Ni (1), Co (2), Mn (3)]

	1	2	3
M1−N1	2.062(3)	2.111(2)	2.250(3)
M1−N2	2.062(3)	2.116(2)	2.247(3)
M1−O1	2.125(2)	2.183(2)	2.258(2)
M1−O3a	2.054(2)	2.051(2)	2.109(2)
M1−O5	2.037(3)	2.063(2)	2.133(2)
M1−O1W	2.052(2)	2.113(2)	2.197(3)
N1−M1−N2	79.6(1)	77.32(7)	72.9(1)
N1−M1−O1	93.3(1)	93.19(6)	91.9(1)
N1−M1−O3a	175.2(1)	173.65(7)	168.8(1)
N1−M1−O5	92.2(1)	92.88(7)	95.3(1)
N1−M1−O1W	87.2(1)	86.46(7)	85.9(1)
N2−M1−O1	90.0(1)	90.34(7)	90.8(1)
N2−M1−O3a	97.3(1)	97.02(7)	95.9(1)
N2−M1−O5	171.6(1)	170.10(7)	168.2(1)
N2−M1−O1W	88.2(1)	88.64(7)	88.67(9)
O1−M1−O3a	90.3(1)	89.69(6)	88.86(9)
O1−M1−O5	92.3(1)	91.54(6)	89.80(9)
O1−M1−O1W	178.1(1)	178.97(6)	177.80(9)
O3a−M1−O5	90.9(1)	92.71(7)	95.80(9)
O3a−M1−O1W	89.1(1)	90.56(7)	93.31(9)
O5−M1−O1W	89.6(1)	89.44(7)	90.30(9)
P1−O4−P2	132.5(2)	131.8(1)	130.3(2)
M1···M1a	5.271(1)	5.3065(8)	5.371(1)
M1···M1b	7.230(1)	7.1633(9)	6.935(2)

[a]Symmetry codes: (a) = $-x + 1, -y + 2, -z + 1$; (b) = $-x + 2, -y + 1, -z + 1$.

RESULTS AND DISCUSSION

Synthesis and Characterization of 1−3. Aqueous solutions of $NiCl_2·6H_2O$ (0.0267 M, 0.0063 g mL^{-1}; **1**), $CoCl_2·6H_2O$ (0.0267 M, 0.0063 g mL^{-1}; **2**), or $MnCl_2·4H_2O$ (0.0267 M, 0.0053 g mL^{-1}; **3**) were treated with solid bipy (0.0267 M, 0.0042 g mL^{-1}) and sodium pyrophosphate (0.0533 M, 0.0142 g mL^{-1}) in a 1:1:2 stoichiometric ratio. The resulting basic solutions were left under continuous stirring for 1 h, and their pH was then adjusted to 2.0 by using 1 M HCl. The acidic solutions were left at room temperature, whereupon crystals formed within 4 (**1**), 1 (**2**), and 3 days (**4**). When the reactions were performed at lower concentrations, the crystal growth time was observed to be significantly lengthened; an effect that could be overcome by heating at 40−60 °C for 24 h prior to standing at room temperature. **1**−**3** can also be prepared by combining the metal hydrate salt with bipy and sodium pyrophosphate in an aqueous solution with a 1:1:1.5 stoichiometic ratio.

Elemental analysis (EA) and thermal analysis (TA) for **3** at a 1:1:2 stoichiometric ratio suggested a less hydrated state than **3** with a molar ratio of 1:1:1.5. The data obtained for **3** at 1:1:2

DOI: 10.1021/acs.inorgchem.5b00866
Inorg. Chem. 2015, 54, 6537−6546

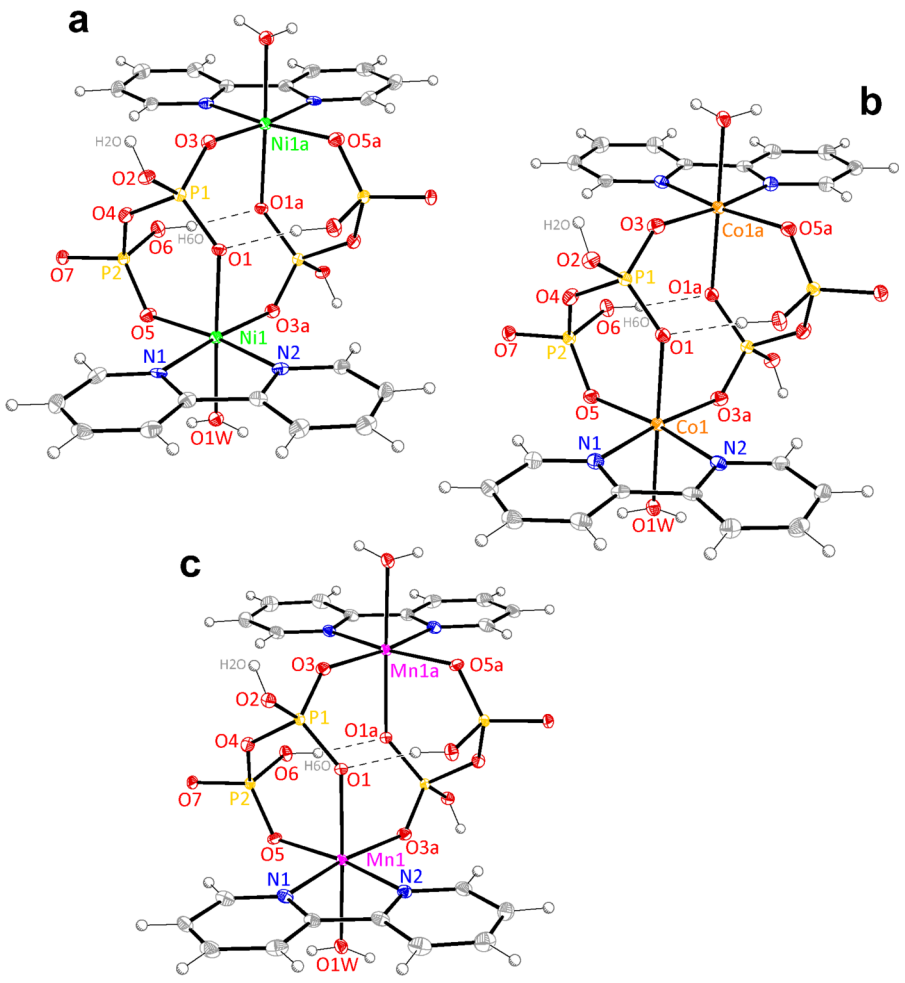

Figure 1. Perspective views of the molecular structures of **1** (a), **2** (b), and **3** (c) along with numbering of the non-carbon atoms. Thermal ellipsoids are drawn at the 50% probability level. Symmetry code: (a) = $-x + 1, -y + 2, -z + 1$.

Table 3. Hydrogen-Bonding Interactions for 1−3[a]

D−H···A	D−H/Å	H···A/Å	D···A/Å	D−H−A/deg
		Compound **1**		
O6−H6O···O1a	0.84	1.76	2.590(3)	170.4
O2−H2O···O7c	0.84	1.77	2.609(3)	174.6
O1W−H1WB···O7e	0.85(2)	1.91(2)	2.732(3)	162(4)
O1W−H1WA···O2Wf	0.85(2)	1.85(2)	2.698(4)	173(4)
O2W−H2WA···O7	0.84(2)	2.05(2)	2.883(4)	171(4)
O2W−H2WB···O5e	0.84(2)	2.52(2)	3.179(4)	136(4)
		Compound **2**		
O6−H6O···O1a	0.84	1.75	2.585(2)	170.3
O2−H2O···O7c	0.84	1.77	2.607(2)	173.8
O1W−H1WB···O7e	0.83(2)	1.94(2)	2.758(2)	166(2)
O1W−H1WA···O2Wf	0.83(2)	1.88(2)	2.700(2)	169(3)
O2W−H2WA···O7	0.83(2)	2.05(2)	2.878(2)	173(3)
O2W−H2WB···O5e	0.84(2)	2.43(2)	3.122(2)	141(2)
		Compound **3**		
O6−H6O···O1a	0.84	1.75	2.572(4)	165.2
O2−H2O···O7c	0.84	1.77	2.604(3)	176.0
O1W−H1WB···O7e	0.82(2)	1.97(2)	2.773(4)	165(5)
O1W−H1WA···O2Wf	0.82(2)	1.89(2)	2.703(4)	173(5)
O2W−H2WA···O7	0.84(2)	2.11(3)	2.900(4)	158(5)
O2W−H2WB···O5e	0.83 (2)	2.17(2)	2.982(3)	167(5)

[a]D = donor and A = acceptor. Symmetry codes used to generate equivalent atoms: (a) = , $-x + 1, -y + 2, -z + 1$; (c) = $-x, -y + 2, -z + 1$; (e) = $-x + 1, -y + 1, -z + 1$; (f) = $x + 1, y, z$.

DOI: 10.1021/acs.inorgchem.5b00866
Inorg. Chem. 2015, 54, 6537−6546

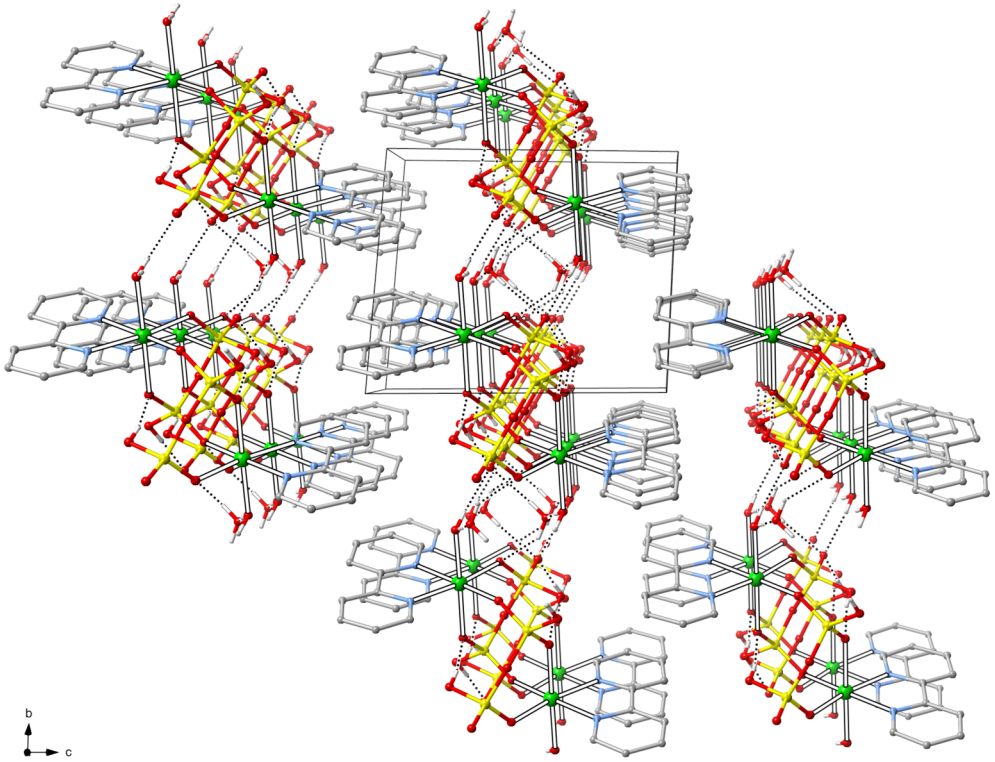

Figure 2. Perspective view of a portion of the crystal packing of **1** along the crystallographic *a* axis. Compounds **2** and **3** show identical packing. Hydrogen bonds are depicted as dotted lines. The hydrogen atoms on the bipy ligands have been omitted for clarity.

correspond to two bound water molecules and the absence of two lattice water molecules. Single-crystal X-ray diffraction confirmed the same structure for **3** at both 1:1:1.5 and 1:1:2, indicating that the discrepancies from EA and TA may be attributed to differences in the number of lattice water molecules.

IR spectroscopy shows the presence of a broad band at ~3400 cm^{-1} typical of lattice water molecules and characteristic bipy (ca. 1600 and 1440 cm^{-1}) and dihydrogenpyrophosphate (several peaks in the range of 1074−1279 cm^{-1}) absorptions. The profile of the IR peaks of the $H_2P_2O_7^{2-}$ ligand in **1**−**3** differs from that observed in the bis-bidentate pyrophosphate,[16,17,19,26−29] suggesting a correlation between the spectroscopic features and the coordination mode adopted by the pyrophosphate ligand in its metal complexes.[19] The IR peaks in **1**−**3** appear shifted (in wavenumbers) from the classic bis-bidentate pyrophosphate moiety but not consistently in one direction (i.e., toward lower or higher wavenumbers). There is no obvious trend to explain the shift of the IR peaks between the two dihydrogenpyrophosphate groups in **1**−**3** and the classic bis-bidentate pyrophosphate. EA coupled with TA results were consistent with the formation of homodinuclear metal(II) complexes of the general formula $[M^{II}(bpy)(H_2P_2O_7)(H_2O)]_2{\cdot}2H_2O$ (**1**−**3**). Single-crystal X-ray diffraction studies confirmed the structural nature.

Description of the Structures of 1−3. The isostructural compounds **1**−**3** crystallize in the triclinic space group $P\bar{1}$. Their structures are made up of centrosymmetric homodinuclear $[M(bpy)(H_2P_2O_7)(H_2O)]_2$ units [M = Ni^{II} (**1**), Co^{II} (**2**), Mn^{II} (**3**); see Figure 1 and Table 2] and crystallization water molecules (two per dimeric unit), which are interlinked by $\pi-\pi$-type interactions and hydrogen bonds (see below).

Each metal(II) ion in **1**−**3** is six-coordinate with two bipy nitrogen atoms (N1 and N2) and two oxygen atoms (O5 and O3a; (a) = $-x + 1, -y + 2, -z + 1$) from two dihydrogenpyrophosphate groups in the equatorial positions, whereas the axial ones are filled by a water molecule (O1W) and a dihydrogenpyrophosphate oxygen (O1), building a somewhat distorted octahedral surrounding. The reduced value of the angle subtended by the chelating bipy at the metal ion [N1−M1−N2 = 79.6(1)° (**1**), 77.32(7)° (**2**), and 72.9(1)° (**3**)] is the main source of this distortion. The metal ion is displaced from the mean equatorial plane by 0.0512(13) Å (**1**), 0.0411(9) Å (**2**), and 0.0093(13) Å (**3**). Two dihydrogenpyrophosphate groups adopting the uncommon bidentate/monodentate coordination modes connect the two divalent metal ions. Two strong intramolecular hydrogen bonds [O6···O1a/O6a···O1; (a) = $-x + 1, -y + 2, -z + 1$; see Table 3] are observed in **1**−**3**, similar to those found in the parent complex $\{[Cu(bipy)(trans\text{-}H_2P_2O_7)]_2\}$.[19] The values of the intramolecular metal−metal separation are 5.2712(9) Å (**1**), 5.3065(7) Å (**2**), and 5.371(1) Å (**3**). These are all shorter than the shortest intermolecular metal−metal separation [7.230(1) Å (**1**), 7.1632(9) Å (**2**), and 6.935(2) Å (**3**) for M1···M1b; (b) = $-x + 2, -y + 1, -z + 1$].

The three-dimensional arrangement of complexes **1**−**3** is shown in Figure 2. Each compound has a variable degree of $\pi-\pi$-stacking interactions and the strongest type of supramolecular interaction, hydrogen bonding.

As shown in Figure 2, the packing of the isostructural homodinuclear units in the crystallographic *ab* plane is driven by hydrogen bonds involving both the coordinated water molecules and the hydrophilic portions of the structure, i.e., the $\{M-(\mu\text{-}H_2P_2O7)_2-M\}$ cores. In particular, each dimer is connected to two symmetry-equivalent ones in the direction of

DOI: 10.1021/acs.inorgchem.5b00866
Inorg. Chem. 2015, 54, 6537−6546

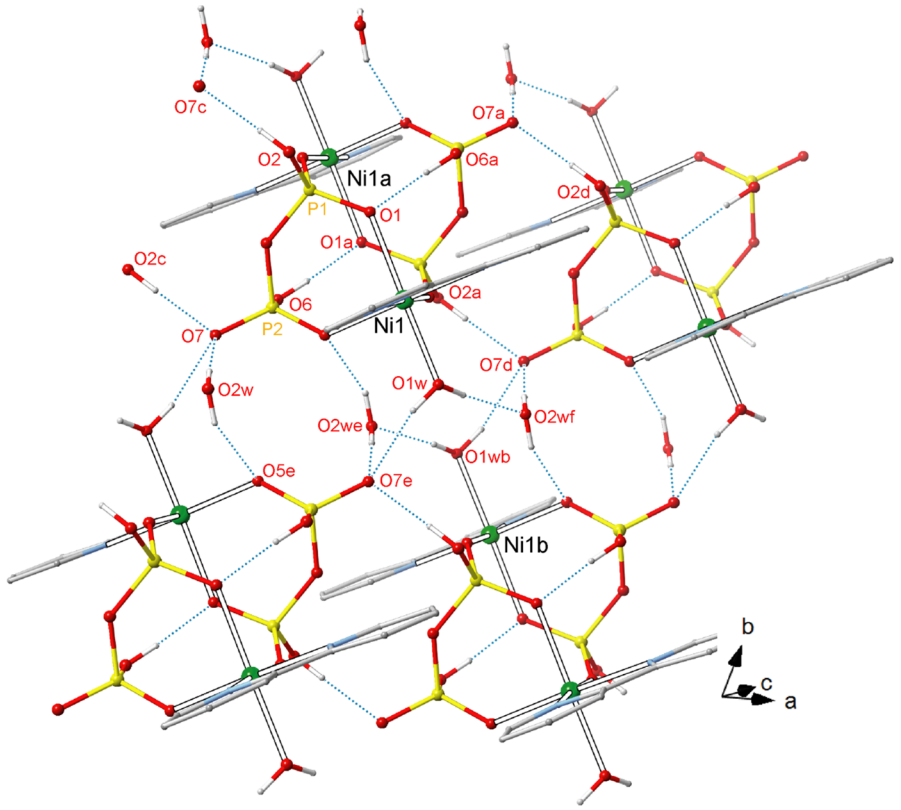

Figure 3. Portion of the hydrogen-bonding pattern in **1** highlighting the interactions listed in Table 3 (dotted lines). An identical pattern is found in **2** and **3**.

the crystallographic *a* axis via two couples of intermolecular hydrogen bonds between vicinal dihydrogenpyrophosphate groups [O2···O7c/O2c···O7 and O2a···O7d/O2d···O7a; (c) = $-x, -y + 2, -z + 1$; (d) = $x + 1, y, z$]. These interactions give rise to supramolecular ribbonlike 1D motifs, interconnected in the [001] direction via an additional strong hydrogen bond involving the dihydrogenpyrophosphate oxygen atom O7 and the coordinated water molecule [O1W···O7e; (e) = $-x + 1, -y + 1, -z + 1$]. The crystallization water molecules, located within the inter-ribbon space, also participate in the stabilization of the resulting 2D supramolecular network by further connecting adjacent ribbons via the dihydrogenpyrophosphate oxygen atoms O5 and O7 as donors and the coordinated water molecule O1W as the acceptor [O2W···O7; O2W···O5e; O1W ···O2Wf; (f) = $x + 1, y, z$]. In **1** and **2**, the O2W···O5e interaction is somewhat loose indeed, although it becomes more effective in **3**. Hydrogen-bond details for **1**−**3** are listed in Table 3, whereas a view of a portion of the described supramolecular layers growing parallel to the *ab* plane in **1**−**3** is given in Figure 3.

Weak interactions due to offset stacking of the bidentate bipy ligands of adjacent dimers are also present within the described ribbon-like motifs, in the direction of the *a* axis, with the interplanar bipy−bipy distances being ca. 3.21 (**1**), 3.23 (**2**), and 3.24 Å (**3**) [*AAAA* arrangement; see Figure 4a]. Additional $\pi-\pi$-stacking interactions are observed along the crystallograhic *b* axis, contributing to the 3D arrangement. These last interactions, which form an "interlayer zipper", are of the *ABAB* type, with the two slightly different interplanar bipy−bipy distances being 3.26/3.34 (**1**), 3.30/3.34 (**2**), and 3.31/3.36 Å (**3**); see Figure 4b.

Thermal Analysis of 1−3. The loss of two water molecules for **1** begins at a temperature of ∼110 °C and starts to level off at 169 °C. This temperature difference accounts for a weight loss of ca. 8.427%. The first inflection point for **2** is ca. 90 °C, and it levels off at 148 °C. The weight loss involved in this process (ca. 8.222%) is consistent with the removal of two noncoordinated water molecules. The loss of two water molecules for **3** begins at a much lower temperature (54 °C) and levels off at 123 °C, accounting for a weight loss of two bound water molecules of ca. 4.942%. The final inflection point in all three complexes is due to a degradation process beginning at ∼371, ∼330, and ∼235 °C for **1**−**3**. The similarities in the structures from the standpoint of crystallographic space group and thermal hydration loss is also manifested in the overall densities calculated crystallographically for **1**−**3**, which are very similar at 1.874 g cm^{-3} (**2**), 1.906 g cm^{-3} (**1**), and 1.806 g cm^{-3} (**3**).

Magnetic Properties of 1−3. For pedagogical reasons, we will focus first on the magnetic properties of **1**, then we will present and analyze those of **2**, and finally we will finish with those of **3**, with this trend following the increasing number of unpaired electrons on each metal center [two, three, and five for high-spin nickel(II), cobalt(II), and manganese(II) ions, respectively].

The magnetic behavior of **1** is shown in Figure 5 in the form of a $\chi_M T$ versus T plot [with χ_M being the magnetic susceptibility per two nickel(II) ions]. $\chi_M T$ at room temperature is 2.38 cm^3 mol^{-1} K, a value that is as expected for two single-ion triplet states magnetically isolated [$\chi_M T$ = 2.42 cm^3 mol^{-1} K with g_{Ni} = 2.20]. This value continuously increases upon cooling to reach a maximum of 2.82 cm^3 mol^{-1} K at 4.5 K and then further decreases to ca. 2.52 cm^3 mol^{-1} K at 1.9 K.

DOI: 10.1021/acs.inorgchem.5b00866
Inorg. Chem. 2015, 54, 6537−6546

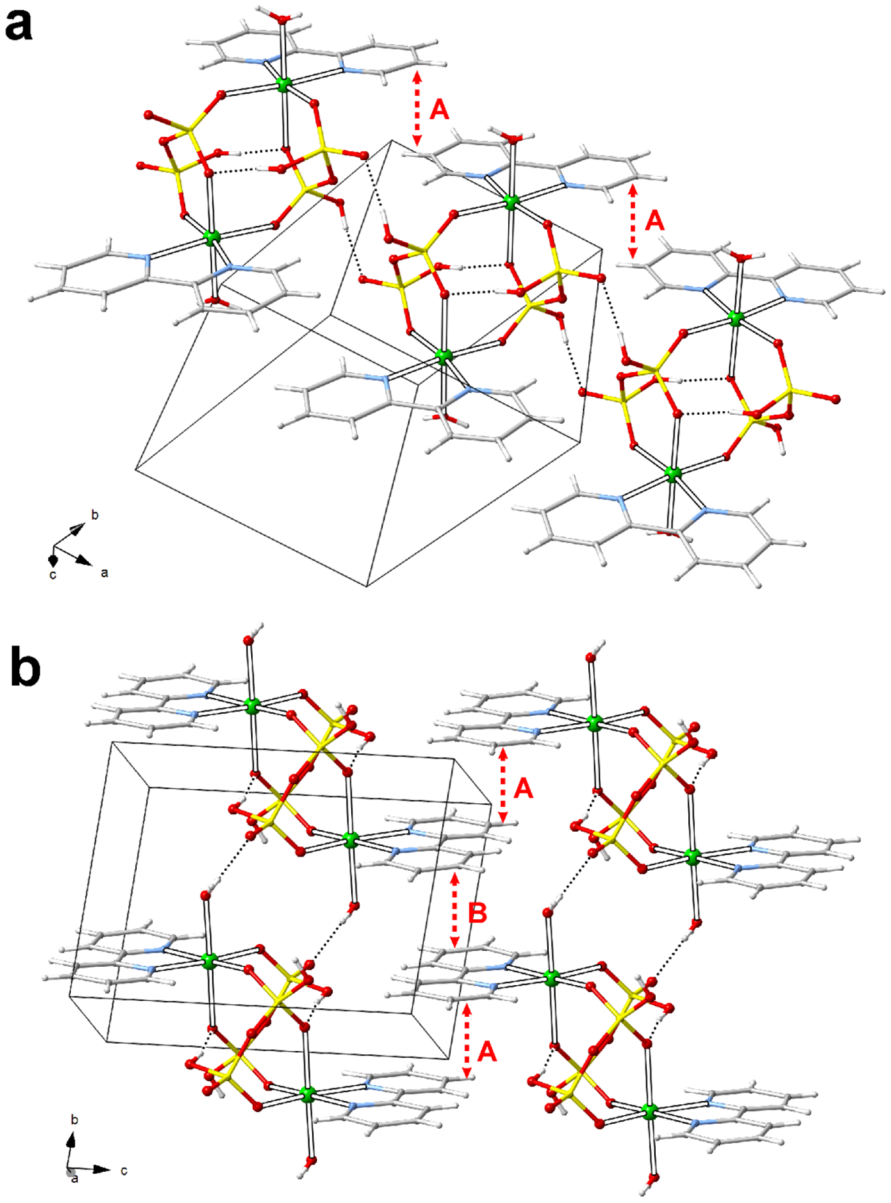

Figure 4. View of the $\pi-\pi$-stacking interactions along the crystallographic a (a; symmetry operation for A = $x + 1$, y, z) and b (b; symmetry operation for A = $-x + 1$, $-y + 1$, $-z + 2$; for B = $-x + 1$, $-y + 2$, $-z + 2$) axes between adjacent bipy ligands in **1**. Crystallization water molecules have been omitted for clarity. Identical hydrophobic motifs are found in **2** and **3**.

The shape of this curve is typical of a weak ferromagnetic interaction in **1**, with the decrease of $\chi_M T$ at very low temperatures being due to zero-field-splitting effects and/or intermolecular antiferromagnetic interactions.

The shape of the magnetization versus H plot at 2.0 K for **1** (see the inset of Figure 5) provides additional support to the occurrence of an intramolecular ferromagnetic interaction: the magnetization at 5 T (maximum value of the applied direct-current field in our magnetometer) is close to 4.0 μ_B (to be compared with the expected saturation value $M_s = gS = 4.40$ μ_B with $g = 2.20$ and $S = 2$). Zero-field-splitting effects would account for the lack of saturation of the magnetization.

Bearing in mind the dinuclear structure of **1** and the fact that the ground state for a six-coordinate nickel(II) ion is orbitally nondegenerate, the isotropic spin Hamiltonian $H = -JS_{Ni1} \cdot S_{Ni1a}$ would account for the intradimer magnetic coupling (J). Nevertheless, this approach only works when a relatively strong antiferromagnetic coupling is involved. In the cases where a weak antiferromagnetic coupling occurs or when the magnetic interaction is ferromagnetic (as in **1**), the effect of the zero-field splitting of the octahedral nickel(II) ions (D) has to be taken into account to describe properly the magnetic behavior at low temperatures.[30] Consequently, we have analyzed the magnetic susceptibility data of **1** in the whole temperature range by the corresponding expression derived through the Hamiltonian of eq 1[30]

$$\boldsymbol{H} = -J\boldsymbol{S}_{Ni1} \cdot \boldsymbol{S}_{Ni1a} + D(\boldsymbol{S}_{z,Ni1}{}^2 + \boldsymbol{S}_{z,Ni1a}{}^2 - 4/3) + g\beta H(\boldsymbol{S}_{Ni1} + \boldsymbol{S}_{Ni1a}) \quad (1)$$

where the first term accounts for the magnetic interaction between the local spin carriers, the second one corresponds to the axial zero-field splitting, and the last term is the Zeeman interaction with $g_{Ni1} = g_{Ni1a} = g$. The best-fit values are $J = +1.86(2)$ cm^{-1}, $D = 3.98(2)$ cm^{-1}, and $g = 2.18(1)$. The

DOI: 10.1021/acs.inorgchem.5b00866
Inorg. Chem. 2015, 54, 6537−6546

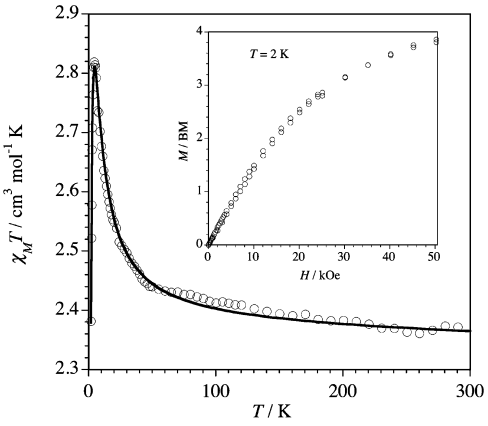

Figure 5. Thermal dependence of the $\chi_M T$ product for **1**: (○) experimental; (—) best-fit curve through eq 1 (see the text). The inset shows the magnetization versus H plot of **1** at 2.0 K.

calculated curve (solid line in Figure 5) matches well the magnetic data in the temperature range explored.

The magnetic properties of **2** in the form of a $\chi_M T$ versus T plot [χ_M is the magnetic susceptibility per two cobalt(II) ions] are shown in Figure 6. At 300 K, $\chi_M T$ is equal to 5.51 cm^3

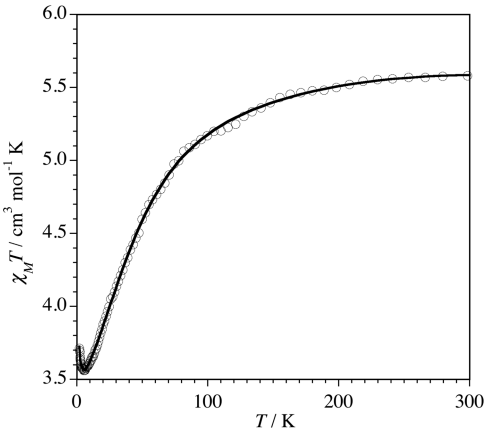

Figure 6. Thermal dependence of the $\chi_M T$ product for **2**: (○) experimental; (—) best-fit curve through eq 2 (see the text).

mol^{-1} K (μ_{eff} per Co^{II} of 4.70 μ_B). Upon cooling, $\chi_M T$ continuously decreases to reach a minimum at 7.0 K (ca. 3.51 cm^3 mol^{-1} K), and it clearly increases at lower temperatures, attaining a value of 3.75 cm^3 mol^{-1} K at 1.9 K. The features allow us to reach conclusions. First, the value of the μ_{eff} per cobalt atom at room temperature for **2** is greater than that expected for the spin-only case (μ_{eff} = 3.87 μ_B with S_{Co} = $^3/_2$), indicating that the distortion of the octahedral geometry of cobalt(II) in **2** is not so large to induce the total quenching of the $^4T_{1g}$ ground state. Second, given that only the Kramers doublet of a high-spin cobalt(II) ion is populated at 1.9 K with an effective spin S_{eff} = $^1/_2$ and a value of the Landé factor g = 4.3,[31,32] the calculated value of $\chi_M T$ for two magnetically isolated spin doublets with this g value is ca. 3.47 cm^3 mol^{-1} K. Because this value is somewhat below that observed for **2** at 1.9 K (3.75 cm^3 mol^{-1} K), there is no doubt of the occurrence of a weak ferromagnetic interaction between the cobalt(II) ions in **2**.

Bearing in mind the dinuclear structure of **2** and the fact that the high-spin six-coordinate cobalt(II) ion is orbitally degenerate, its magnetic properties can be appropriately described by using the Hamiltonian of eq 2[33]

$$\begin{aligned} \boldsymbol{H} = &-J\boldsymbol{S}_{Co1}\cdot\boldsymbol{S}_{Co1a} - \alpha\lambda(\boldsymbol{L}_{Co1}\cdot\boldsymbol{S}_{Co1} + \boldsymbol{L}_{Co1a}\cdot\boldsymbol{S}_{Co1a}) \\ &+ \Delta(\boldsymbol{L}_{Co1} + \boldsymbol{L}_{Co1a} - 4/3) + \beta H[-\alpha(\boldsymbol{L}_{Co1} + \boldsymbol{L}_{Co1a}) \\ &+ 2(\boldsymbol{S}_{Co1} + \boldsymbol{S}_{Co1a})] \end{aligned} \quad (2)$$

which includes four terms: (a) the isotropic exchange coupling between the two local spin quartets (S_{Co1} = S_{Co1a} = $^3/_2$); (b) the spin−orbit coupling of the $^4T_1$ ground term in octahedral symmetry; (c) the splitting of the T_1 orbital term into a singlet and a doublet orbital terms (with Δ being the energy gap) due to axial symmetry; (d) the Zeeman interaction. λ is the spin−orbit coupling parameter, α is an orbital reduction factor defined as $\alpha = A\kappa$, where κ considers the reduction of the orbital momentum caused by delocalization of the unpaired electrons and A is a crystal-field parameter (A = $^3/_2$ and 1 for weak and strong crystal-field limits, respectively). In the frame of T_1 and P term isomorphism, $\boldsymbol{L}(T_{1g}) = -A\boldsymbol{L}(P)$, one can use L = 1 and treat the term $\alpha\lambda\boldsymbol{L}\cdot\boldsymbol{S}$ as an isotropic Hamiltonian describing the interaction between the two angular momenta L = 1 and S = $^3/_2$, with AL being the coupling parameter and the term in eq 2 as a zero-field splitting of the angular momentum L = 1. A least-squares fit of the magnetic susceptibility data of **2** through this approach leads to the following values: J = +0.25(1) cm^{-1}, α = 1.23(1), λ = 140(2) cm^{-1}, and Δ = 510(5) cm^{-1}. The calculated curve (solid line in Figure 6) reproduces well the magnetic data over the whole temperature range.

The magnetic properties of **3** in the form of a $\chi_M T$ versus T plot [χ_M is the magnetic susceptibility per two manganese(II) ions] are shown in Figure 7. At 300 K, $\chi_M T$ is equal to 8.70 cm^3

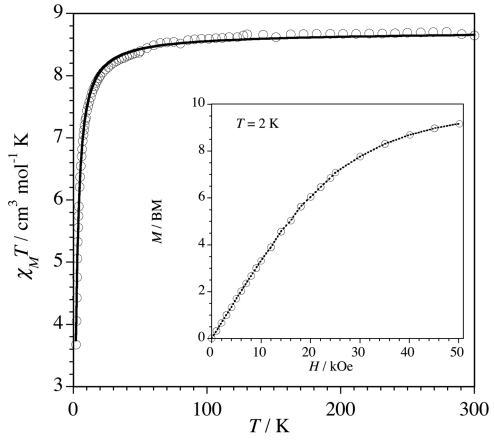

Figure 7. Thermal dependence of the $\chi_M T$ product for **3**: (○) experimental; (—) best-fit curve through eq 3 (see the text). The inset shows the M versus H plot for **3** at 2.0 K (the dotted line is an eye-guide).

mol^{-1} K, a value that is as expected for two magnetically noninteracting sextuplet spin states [$\chi_M T$ = 8.75 cm^3 mol^{-1} K with S_{Mn} = $^5/_2$ and g_{Mn} = 2.0]. Upon cooling, $\chi_M T$ remains practically constant down to 100 K, and it further decreases to reach a value of 3.68 cm^{-1} mol^{-1} K at 1.9 K. This plot is typical of a weak antiferromagnetic coupling between the manganese(II) ions in **3**, a feature that receives additional support by the shape of the magnetization versus H plot at 2.0 K (see the inset of Figure 7).

DOI: 10.1021/acs.inorgchem.5b00866
Inorg. Chem. 2015, 54, 6537−6546

In agreement with the dinuclear structure of **3**, its magnetic susceptibility data were analyzed in terms of an isotropic exchange interaction through the Hamiltonian $\boldsymbol{H} = -J\boldsymbol{S}_{Mn1}\cdot\boldsymbol{S}_{Mn1a}$ by using eq 3

$$\chi_M = (2N\beta^2g^2/kT)\{[x + 5x^3 + 14x^6 + 30x^{10} + 55x^{15}] /[1 + 3x + 5x^3 + 7x^6 + 9x^{10} + 11x^{15}]\} \quad (3)$$

where N, β, and g have their usual meanings and $x = \exp(J/kT)$. Least-squares best-fit parameters are $J = -0.48(1)$ cm^{-1} and $g = 1.99(1)$. There is a good match between the calculated curve and the magnetic data in the whole temperature range investigated.

We would like to finish the present contribution with a discussion about the values and nature of the magnetic interactions between the divalent metal ions through the double −O−P−O− and −O−P−O−P−O− bridging pathways in **1**−**3** (see Scheme 2), which are ferromagnetic [J = +1.86 cm^{-1} (**1**) and +0.25 cm^{-1} (**2**)] and antiferromagnetic [J = −0.48 cm^{-1} (**3**)].

Scheme 2. Structural Drawing Showing the Equatorial−Axial Connection through Each M−O−P−O−M Arm in 1 (M = Ni), 2 (M = Co), and 3 (M = Mn)

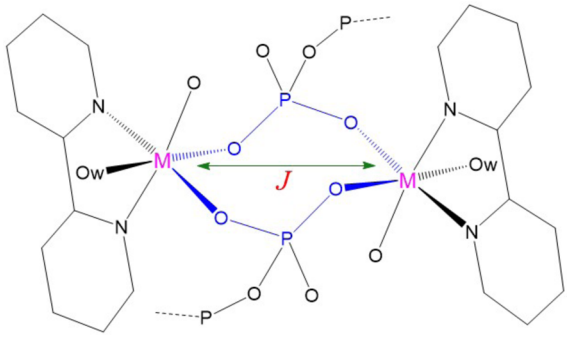

Simple orbital symmetry considerations allow us to understand the variation of the magnetic coupling in **1**−**3**. Six-coordinate nickel(II) (electronic configuration $t_{2g}^6e_g^2$ in O_h symmetry) has two unpaired electrons, which are described by the $d_{x^2-y^2}$- and d_{z^2}-type orbitals (the x and y axes are defined by the Ni1−N_{bpy} bonds being located in the equatorial plane and the z axis by the O1W−Ni1−O1 vector corresponding to the axial positions; see Scheme 2). Although there are two bridging pathways (double −O−P−O− and −O−P−O−P−O− arms), the main contribution to the magnetic exchange would be provided by the shorter one, which connects one equatorial position at one metal ion with an axial one at the other metal center in the centrosymmetric dinickel(II) compound. For such a situation, the orthogonality between the $d_{x^2-y^2}$ and d_{z^2} magnetic orbitals of adjacent nickel(II) ions is predicted, and then a ferromagnetic interaction would result, as observed. This analysis is also valid for the isostructural compounds **2** and **3** but the increasing number of unpaired electrons on each metal center when going from nickel(II) to cobalt(II) to manganese(II) introduces significant changes. Each high-spin cobalt(II) in **1** has three unpaired electrons ($t_{2g}^5e_g^2$ electronic configuration) versus two for the nickel(II) ion in **1**. It is well established that when the number of unpaired electrons on the interacting metal centers is different, everything being equal, the net magnetic coupling is not properly described by J but by n_An_BJ, with n_A and n_B being the number of unpaired electrons on each metal center [$n_A = n_B = 2$ (nickel(II)) and 3 (cobalt(II)) in the homodinuclear compounds **1** and **2**, respectively].[34] The values of n^2J obtained then, +2.25 cm^{-1} (**2**) and +7.24 cm^{-1} (**1**), suggest the occurrence in **2** of additional antiferromagnetic contributions arising from the t_{2g} unpaired electron at each cobalt(II) ion. These antiferromagnetic contributions are expected to be even more important in the case of **3** where five unpaired electrons occur (electronic configuration $t_{2g}^3e_g^2$, $n = 5$). Accordingly, the value of n^2J for **3** becomes negative (−12 cm^{-1}), with the antiferromagnetic terms provided by the t_{2g}−t_{2g} combinations overcoming the ferromagnetic ones from the $d_{x^2-y^2}$−d_{z^2} pairs.

CONCLUSIONS

Three isostructural coordination complexes containing a double-bridged dihydrogenpyrophosphate moiety are synthesized and structurally, thermally, and magnetically characterized. Single-crystal X-ray diffraction shows crystal structures **1**−**3** as triclinic, crystallizing in the space group $P\bar{1}$. Magnetic interactions occur between the divalent metal centers through the double −O−P−O− bridging pathway. Analysis of the magnetic data shows a rare phenomenon of two ferromagnetic compounds containing a double-bridged dihydrogenpyrophosphate moiety, $[Ni(bipy)(H_2P_2O_7)(H_2O)]_2\cdot 2H_2O$ (**1**; J = +1.86 cm^{-1}) or $[Co(bipy)(H_2P_2O_7)(H_2O)]_2\cdot 2H_2O$ (**2**; J = +0.25 cm^{-1}), and one classic antiferromagnetic interaction for $[Mn(bipy)(H_2P_2O_7)(H_2O]_2\cdot 2H_2O$ (**3**; J = −0.48 cm^{-1}). To date, only one other compound containing a double-bridged dihydrogenpyrophosphate moiety of the formula $\{[Cu(bipy)(cis\text{-}H_2P_2O_7)]_2\}\cdot 3H_2O$ (**4**) has been magnetostructurally characterized, and it exhibits an intramolecular ferromagnetic coupling [J = +0.86(1) cm^{-1}].[19] The magnetostructural study of **1**−**3**, combined with **4**, shows that the nature of the magnetic interaction across a double dihydrogenpyrophosphate bridge can vary from ferro- to antiferromagnetic depending on the nature of the metal ion of the homodinuclear species.

ASSOCIATED CONTENT

Supporting Information

X-ray crystallographic data in CIF format. The Supporting Information is available free of charge on the ACS Publications website at DOI: 10.1021/acs.inorgchem.5b00866.

AUTHOR INFORMATION

Corresponding Authors

*E-mail: Miguel.julve@uv.es.
*E-mail: rpdoyle@syr.edu.

Present Addresses

⊥A.G.G.: Department of Physics, University of Texas at El Paso, El Paso, Texas 79968, United States.
§N.M.: Istituto per la Tecnologia delle Membrane, ITM-CNR, Via Pietro Bucci, Cubo 17C, c/o Campus of University of Calabria, 87036 Rende (CS), Italy.

Notes

The authors declare no competing financial interest.

ACKNOWLEDGMENTS

R.P.D. thanks the American Chemical Society (DNI award 48999-DNI 3), the iLEARN and Renee Crown Honors programs at Syracuse University, and the National Science Foundation (for the purchase of a single-crystal X-ray

DOI: 10.1021/acs.inorgchem.5b00866
Inorg. Chem. 2015, 54, 6537−6546

diffractometer) for funding. Financial support from the Ministerio Español de Economía y Competitividad (Project CTQ2013-44844P) is also acknowledged.

REFERENCES

(1) Terkeltaub, R. A. *Am. J. Physiol. Cell Physiol.* **2001**, *281*, C1−C11.
(2) *Inorganic Polyphosphate: A Molecule of Many Functions*; Kornberg, A., Ed.; Springer-Verlag: Berlin, 1999.
(3) (a) *The Biochemistry of Nucleic Acids*, 10th ed.; Adams, R. L. P., Knowler, J. T., Leader, D. P., Eds.; Chapman and Hall: New York, 1986. (b) Boyer, P. D. *Angew. Chem., Int. Ed.* **1998**, *37*, 2296−2307.
(4) Doyle, R. P.; Nieuwenhuyzen, M.; Kruger, P. E. *Dalton Trans.* **2005**, 3745−3750 and references cited therein.
(5) Ikotun, O. F.; Higbee, E. M.; Ouellette, W.; Doyle, R. P. *J. Inorg. Biochem.* **2009**, *103*, 1254−1264 and references cited therein.
(6) *Biochemistry*; Metzler, D. E., Ed.; Elsevier Science: San Diego, 2003; Vol. *2*.
(7) Kornberg, A.; Rao, N. N.; Ault-Riché, D. *Annu. Rev. Biochem.* **1999**, *68*, 89−125.
(8) Foster, B. L.; Nagatomo, K. J.; Nociti, F. H., Jr.; Fong, H.; Dunn, D.; Tran, A. B.; Wang, W.; Narisawa, S.; Millan, J. L.; Somerman, M. J. *PLoS One* **2012**, *7*, e38393.
(9) Villa-Bellosta, R.; Wang, X.; Millan, J. L.; Dubyak, G. R.; O'Neill, W. C. *Am. J. Physiol. Heart Circ. Physiol.* **2001**, *301*, H61−H68.
(10) Fleisch, H.; Schibler, D.; Maerki, J.; Frossard, I. *Nature* **1965**, *207*, 1300−1301.
(11) *Inorganic Chemistry in Biology*; Wilkins, P. C.,Wilkins, R. G., Eds.; Oxford University Press: New York, 1997.
(12) Jansen, R. S.; Kucukosmanoglu, A.; de Haas, M.; Sapthu, S.; Otero, J. A.; Hegman, I. E. M.; Bergen, A. A. B.; Gorgels, T. G. M. F.; Borst, P.; van de Wetering, K. *Proc. Natl. Acad. Sci. U.S.A.* **2013**, *110*, 20206−20211.
(13) Ikotun, O. F.; Marino, N.; Kruger, P. E.; Julve, M.; Doyle, R. P. *Coord. Chem. Rev.* **2010**, *254*, 890−915.
(14) Sabiah, S.; Varghese, B.; Murthy, N. N. *Chem. Commun.* **2009**, 5636−5638.
(15) Hoffman, A. E.; Marino, N.; Lloret, F.; Julve, M.; Doyle, R. P. *Inorg. Chim. Acta* **2012**, *389*, 151−158.
(16) Kruger, P. E.; Doyle, R. P.; Julve, M.; Lloret, F.; Nieuwenhuyen, M. *Inorg. Chem.* **2001**, *40*, 1726−1727.
(17) Ikotun, O. F.; Ouellette, W.; Lloret, F.; Kruger, P. E.; Julve, M.; Doyle, R. P. *Eur. J. Inorg. Chem.* **2008**, 2691−2697.
(18) Sartoris, R. P.; Nascimento, O. R.; Santana, R. C.; Perec, M.; Baggio, R. F.; Calfo, R. *Dalton Trans.* **2014**, *00*, 1−12.
(19) Marino, N.; Ikotun, O. F.; Julve, M.; Lloret, F.; Cano, J.; Doyle, R. P. *Inorg. Chem.* **2011**, *50*, 378−389.
(20) Earnshaw, A. *Introduction to Magnetochemistry*; Academic Press: London, 1968.
(21) *APEX2*, version 2014.7-1; Bruker AXS: Madison, WI, 2014.
(22) *SAINT*, version 6.45; Bruker Analytical X-ray Systems Inc.: Madison, WI, 2003.
(23) *SADABS*, version 2.03; Bruker AXS Inc.: Madison, WI, 2000.
(24) Sheldrick, G. M. *TWINABS*; University of Göttingen: Göttingen, Germany, 1996.
(25) Sheldrick, G. M. *Acta Crystallogr., Sect. A: Found. Crystallogr.* **2008**, *64*, 112−122.
(26) Ikotun, O. F.; Armatus, N. G.; Julve, M.; Kruger, P. E.; Lloret, F.; Nieuwenhuyzen, M.; Doyle, R. P. *Inorg. Chem.* **2007**, *46*, 6668−6674.
(27) Marino, N.; Mastropietro, T. F.; Armentano, D.; De Munno, G.; Doyle, R. P.; Lloret, F.; Julve, M. *Dalton Trans.* **2008**, *38*, 5152−5154.
(28) Ikotun, O. F.; Higbee, E. M.; Ouelette, W.; Lloret, F.; Julve, M.; Doyle, R. P. *Eur. J. Inorg. Chem.* **2008**, *33*, 5281−5286.
(29) *Infrared and Raman Spectra of Inorganic and Coordination Compounds, Part B, Applications in Coordination, Organometallic and Bioinorganic Chemistry*, 5th ed.; Nakamoto, K., Ed.; John Wiley: New York, 1997.
(30) De Munno, G.; Julve, M.; Lloret, F.; Derory, A. *J. Chem. Soc., Dalton Trans.* **1993**, 1179.
(31) Carlin, R. L. *Magnetochemistry*; Springer-Verlag: Berlin, 1986.
(32) (a) Herrera, J. M.; Bleuzen, A.; Dromzée, Y.; Julve, M.; Lloret, F.; Verdaguer, M. *Inorg. Chem.* **2003**, *42*, 7052. (b) Rodríguez, A.; Sakiyama, H.; Masciocchi, N.; Gálvez, N.; Lloret, F.; Colacio, E. *Inorg. Chem.* **2005**, *44*, 8399. (c) Mishra, V.; Lloret, F.; Mukherjee, R. *Inorg. Chim. Acta* **2006**, *359*, 4053.
(33) Lloret, F.; Julve, M.; Cano, J.; Ruiz-García, R.; Pardo, E. *Inorg. Chim. Acta* **2008**, *361*, 3432.
(34) (a) Kahn, O. *Molecular Magnetism*; VCH Publishers: Weinheim, Germany, 1993; p 186. (b) Kahn, O. *Struct. Bonding (Berlin)* **1987**, *68*, 89. (c) Kahn, O.; Tola, P.; Coudanne, H. *Chem. Phys.* **1979**, *42*, 355. (d) Tola, P.; Kahn, O.; Chauvel, C.; Coudanne, H. *Nouv. J. Chim.* **1979**, *1*, 467.

DOI: 10.1021/acs.inorgchem.5b00866
Inorg. Chem. 2015, 54, 6537−6546